J Soils Sediments (2018) 18:1303–1313
DOI 10.1007/s11368-016-1595-y

Selective effects of forest fires on the structural domains of soil humic acids as shown by dipolar dephasing ^{13}C NMR and graphical-statistical analysis of pyrolysis compounds

Gonzalo Almendros[1] · Pilar Tinoco[2] · José-María De la Rosa[3] · Heike Knicker[3] · José-Antonio González-Pérez[3] · Francisco J. González-Vila[3]

Received: 7 June 2016 / Accepted: 1 November 2016 / Published online: 16 November 2016

Abstract
Purpose Data management strategies of pyrolysis results and NMR acquisition modes were examined in humic acids (HAs) from control soils and fire-affected soils. The information supplied by dipolar dephasing (DD) ^{13}C NMR spectroscopy and Curie-point pyrolysis were used to assess chemical structures hardly recognizable and measurable, or of unclear interpretation, when using ^{13}C NMR under standard acquisition pulses (cross-polarization/magic angle spinning, CPMAS).
Materials and methods The HAs were isolated from two forest soils under *Pinus halepensis* and *Pinus sylvestris* in control and burned sites affected by medium or severe-intensity wildfires. For NMR analyses, during DD acquisition conditions, a 180° ^{13}C pulse was inserted to minimize phase shifts. Curie-Point pyrolysis was carried out at 510 °C for 5 s, and the pyrolysis fragments were analyzed by GC/MS. The total abundances of the major pyrolysis products were compared by an update of the classical Van Krevelen's graphical-statistical approach, i.e., as surface density values in the space defined by the compound-specific H/C and O/C atomic ratios.
Results and discussion The DD ^{13}C NMR experiments displayed significant differences in the HA spectral profiles as regards to the standard CPMAS ^{13}C NMR acquisition conditions, mainly in the chemical shift region of alkyl structures as well as for tannin- or carbohydrate-like *O*-alkyl structures. In fact, the comparison between DD and CPMAS solid-state NMR suggested shortening of alkyl chains and generation of carbohydrate-derived, unsaturated structures—viz. furans—which adds to the aromatic domain. Pyrolytic results showed fire-induced specific changes in HAs chemical structure and its molecular diversity. The changes were evident in the location and sizes of the different clusters of pyrolysis compounds defined by their atomic ratios.
Conclusions The DD ^{13}C NMR provided specific information on the fate of aliphatic structures and the origin of unsaturated HA structures, which could be helpful in differentiating "inherited" from "pyrogenic" aromatic structures. This is further confirmed by the analysis of the molecular assemblages of pyrolytic products, which showed accumulation of condensed polyaromatic domains in the HAs after the high-intensity fire, accompanied by a recalcitrant alkyl hydrocarbon domain. Medium-intensity fire led to aromaticity increase due to a selective accumulation of lignin-derived phenols concomitant to the depletion of aliphatic hydrocarbon constituents.

Keywords Curie-point pyrolysis · Dipolar dephasing · Forest fires damage levels · Humic acid structural changes · NMR

Responsible editor: Claudio Zaccone

Electronic supplementary material The online version of this article (doi:10.1007/s11368-016-1595-y) contains supplementary material, which is available to authorized users.

✉ Gonzalo Almendros
humus@mncn.csic.es

[1] MNCN (CSIC), Serrano 115, 28006 Madrid, Spain

[2] University Alfonso X el Sabio, Villanueva de la Cañada. Av. Universidad 1, 28691 Madrid, Spain

[3] Instituto de Recursos Naturales y Agrobiología de Sevilla (IRNAS-CSIC), Avda. Reina Mercedes 10, 41012 Seville, Spain

1 Introduction

The analytical potential of non-destructive techniques in providing qualitative and quantitative structural information when applied to complex heterogeneous macromolecular materials has

been widely recognized (Stevenson 1994 and references therein). In fact, in the last decades, solid-state NMR spectroscopy has established itself as a reliable non-destructive tool for analyzing chemically complex macromolecular structures in soil, such as those in humic fractions. However, even assuming optimum acquisition conditions, the interpretation of solid-state NMR spectra remains difficult (Wilson 1987). This is mainly due to (a) the overlapping of signals from the numerous C-types in complex macromolecular structures (e.g., in protein-like structures, alkyl, carbonyl, or methoxyl groups) or to (b) the ambiguous signal assignations (e.g., aromatic vs. unsaturated alkyl structures). An elegant approach to reduce the problem of peak overlap is the use of dipolar dephasing conditions which allows to distinguish between C groups with strong and weak dipolar interactions with the proton spin system (Alemany et al. 1983; Knicker 2011).

In this work, we take advantage of the supplementary information provided by DD ^{13}C NMR on chemical structures that frequently produce signals of unclear interpretation when obtained with standard ^{13}C NMR acquisition pulses (Smernik and Oades 2001; Czimczik et al. 2002; Conte et al. 2004). This technique was applied in the 1980s to study lignins and HAs from volcanic soils (Hatcher 1987; Hatcher et al. 1989). In particular, DD ^{13}C NMR could result particularly responsive to the structural arrangement of aromatic structures in soil HAs, i.e., their average degree of protonation (Wilson 1987), which is an important issue in soils subjected to the impact of fires. In particular, it has been indicated that an enhancement in HAs aromaticity occurs in fire-affected soils (González-Pérez et al. 2004) due to two simultaneous processes: (i) concentration of defunctionalized, preexisting aromatic structures of high resistance to thermal degradation compared to the aliphatic soil organic matter constituents and, (ii) thermal rearrangement of aliphatic constituents (mainly carbohydrate-like) leading to newly-formed unsaturated (anhydrosugars, furans) and aromatic (including polycyclic) compounds. In particular, the balance of aromaticity could be considered an index surrogate for fire intensity (Almendros and González-Vila 2012), which cannot be easily expressed in terms of the concentration of pyrogenic structures since it has been demonstrated that DD relaxation times of black carbon standards are substantially the same than those for biogenic aromatic C-forms in fire-unaffected soils (Knicker et al. 2005; Knicker 2007), suggesting that pyrogenic structures are less condensed as commonly assumed. In fact, the parallel monitoring with degradation techniques such as Py-GC/MS (also considered a convenient tool to release meaningful structural fragments from C–C bonded, chemically recalcitrant materials) is convenient to provide complementary chemical structural information.

Nevertheless, due to the well-known limitations of degradation techniques to yield unbiased quantitative results, in this paper, the pyrolytic molecular assemblages will not be discussed from numerical values, but approached from a visual inspection of plots where compounds of similar stoichiometry appear as overlapped clusters. The sizes of such clusters would depend both on the population density and the total abundances of the individual pyrolysis molecules when represented in simple discriminant axes (i.e., the H/C and O/C atomic ratios) defining well-known biogeochemical structural gradients (van Krevelen 1950).

2 Materials and methods

2.1 Sampling

Two forest soils under *Pinus halepensis* and *Pinus sylvestris* were sampled in control, in unaltered sites (labeled as F1, F3, respectively), and in neighbor burned sites (F2, F4). The control soil plot and its burned counterpart had similar characteristics (Table 1). In the burned sites, the pine vegetation was completely removed either by severe (F2) or medium-intensity wildfires (F4). Sampling was carried out in duplicate; composite samples of five subsamples were collected after

Table 1 Characteristics of the sampling sites in control and post-fire forest soils at Central Spain

Sample	Fire intensity	Altitude m asl	Slope %	Soil type[a]	Location	Vegetation	UTM	Geological substrate
F1	None	630	0	Calcaric Cambisol (Loamic, Humic)	Road from Perales del Río to San Martín de la Vega (Madrid)	*Pinus halepensis*	4460–400	Limestone
F2	High	624	8	Calcaric Cambisol (Loamic, Humic)	Road from Perales del Río to San Martín de la Vega (Madrid), 100 m apart from F1	Removed by fire (herbaceous)	4460–400	Limestone
F3	None	1580	20	Cambic Umbrisol (Loamic, Hyperdystric)	Puerto de Somosierra (Madrid)	*Pinus sylvestris* (reafforested)	4550–450	Gneiss
F4	Medium	1615	15	Hyperdystric Cambisol (Loamic, Humic)	Puerto de Somosierra (Madrid), 1.5 km apart from F3	Herbaceous (charred trunks of *Pinus sylvestris)*	4550–450	Gneiss

[a] World Reference Base for Soil Resources 2006

removing the litter layer, when existing, and the soil material (O horizon) was collected with a spade. The samples were air-dried; large organic and mineral fragments were removed manually, and the soil sample was homogenized and sieved to fine earth (2 mm).

2.2 Soil general analyses

Table 2 summarizes the main analytical characteristics of the soils. A 1:2.5 soil-to-water suspension was used for pH measurements; the N was determined by micro-Kjeldahl digestion. Available K, Ca, and Mg were extracted with 1 *M* NH_4OAc (pH = 7), and its concentration was determined by an atomic absorption spectroscopy. The effective cation exchange capacity was calculated as the sum of the exchangeable acidity and the 1 *M* NH_4OAc exchangeable cations. Soil oxidizable C was determined by a wet oxidation with the Walkley and Black (1934) method.

2.3 Extraction of HAs

The HAs were isolated after the previous physical removal of the particulate soil fraction with plant remains (free organic matter) by flotation in a 1.8-kg m^{-3} $CHBr_3$-MeOH mixture and centrifugation (Monnier et al. 1962). The resulting soil pellet was desiccated at 40 °C, grounded and extracted with 0.1 *M* $Na_4P_2O_7$, followed by 0.1 *M* NaOH, five times each (Duchaufour 1987). The brownish supernatant solution (i.e., the total humic extract) was precipitated by a dropwise addition of 6 *M* HCl leading to insoluble HAs, which were dialyzed in cellophane bags and desiccated on Petri dishes at 40 °C.

2.4 Solid-state CPMAS-NMR spectroscopy of the HAs

The solid-state ^{13}C–NMR spectra were acquired with a Bruker MSL 100 (2.3 Tesla) at 25.1 MHz, and the CPMAS was performed at 4 kHz. Between 10,000 and 90,000 free induction decays per spectrum were accumulated. The pulse repetition rate was 0.5 s with a contact time of 1 ms. The chemical shift of the NMR spectra was referred to tetramethylsilane (= 0 ppm) using external glycine as standard (176.03 ppm). It was considered that these conditions provide reliable quantitative integration values in the different spectral regions (Fründ and Lüdemann 1989). Concerning DD NMR acquisition conditions, the spectra were obtained with the same amount of scans, introducing a delay time (DD time) of 60 ms before acquisition. During the DD, a 180° ^{13}C pulse was inserted to minimize phase shifts (Hatcher 1987; Hatcher et al. 1989).

2.5 Pyrolysis-gas chromatography-mass spectrometry

The HAs were subjected to Curie-point pyrolysis using a Horizon Instruments pyrolysis unit connected to a Varian Saturn 2000 GC/MS system. The samples deposited on ferromagnetic wires were heated at 510 °C for 5 s. The temperature of the interface of the pyrolysis unit was set to 250 °C, and the gas chromatograph was programmed from 50 to 100 °C at 32 °C min^{-1} and then up to 320 °C at a rate of 6 °C min^{-1}. The injection port was attached to a cryogenic unit cooled with liquid CO_2 and programmed from −30 °C (1 min) to 300 °C at 20 °C min^{-1}. A fused-silica column (25 m × 0.32 mm × 0.4 μm) coated with CPSil was used.

Tentative assignation of the structure of the pyrolytic compounds was carried out from their electron impact mass spectra (70 eV) and also based on the retention times of the main series of homologous compounds, after monitoring the selected ion traces in the reconstructed ion chromatograms.

The peak area (total area counts) of the pyrograms was integrated for the different compounds and calculated as total abundances (excluding presumptively contaminant compounds and minor compounds representing less than 0.5 % of the total chromatographic area). Pyrolysis compounds in the four samples were essentially similar, and in order to build up plots showing at first sight the semiquantitive differences between the four scenarios studied, the method devised was plotting "surface density plots" from the total abundances of the molecules in the space defined by their H/C and O/C ratios. This method represents an updating of the intuitive classical Van Krevelen (1950) graphical-statistical method, very useful to identify molecular changes in the course of e.g., coalification or humification processes. In fact, such an approach has been routinely used to simplify the interpretation

Table 2 Analytical characteristics of soil samples (0–10 cm depth)

Sample	pH in H_2O	Sand g kg^{-1}	Silt g kg^{-1}	Clay g kg^{-1}	C g kg^{-1}	C/N ratio	CEC $cmol_c kg^{-1}$	S $cmol_c kg^{-1}$
F1 (control)	6.9	344	536	120	213	14.5	70.6	49.7
F2 (burnt)	8.7	534	341	125	39	12.3	13.5	13.5
F3 (control)	4.6	603	320	77	69	14.7	23.5	2.1
F4 (burnt)	5.7	646	290	64	64	8.2	41.2	4.0

CEC cation exchange capacity, *S* sum of exchangeable bases ($Na^+ + K^+ + Ca^{2+} + Mg^{2+}$)

Sample labels refer to the "Materials and methods" section

of the very large number of ions released by a Fourier transform ion cyclotron resonance mass spectrometry (e.g., Kramer et al. 2004). In this case, the atomic H/C and O/C ratios of the pyrolysis compounds were represented in the basal plane (*x*,*y* axes) whereas the vertical dimension (*z* axis) corresponded to the total abundances. By using the authors' own ad hoc computer program, the original $z(x, y)$ vectors were transferred into a 50 × 50 matrix (suitable to reallocate the 103 individual compounds represented in the new space defined by the atomic ratios) by an agglomerative manner (i.e., the total abundance values *z* were summed when overlapping in cells of the discrete plane defined by the 50 × 50 matrix with the atomic ratios). In a second stage, up to three iterations of the moving average algorithm (i.e., averaging four neighbor cells together with each central cell) was used to interpolate neighbor *z* values to yield a density surface. Despite the limitations of surface plots for comparing multiple samples, the differences between pairs of samples (e.g., F1 vs F2 or between the unburnt F1, F3 samples) may be graphically displayed as subtraction surfaces with peaks and valleys, in this case, illustrating concentration or selective depletion of the constituents of structural domains of different thermal resistance (Electronic Supplementary Material).

3 Results and discussion

3.1 Solid-state CPMAS-NMR spectroscopy of the HAs

Figure 1 shows the comparison of the solid-state ^{13}C NMR spectra of the HAs from the two soil plots before and after the wildfires acquired with CPMAS conditions, as well as their counterparts obtained with the DD pulse sequence. For more straightforward quantitative comparison, the DD spectra and CPMAS spectra were scale-adjusted to the 172 ppm peak, since the corresponding carbonyl carbons are typically non-protonated, and their intensity should only be slightly affected after a dipolar dephasing time of 60 μs.

Up to four main spectral regions were integrated corresponding to different C-types: alkyl C (0–46 ppm), *O/N*-alkyl C (46–110 ppm), aromatic C (110–160 ppm), and carbonyl C (160–220 ppm) (Table 3). A series of subregions were also integrated independently (Table 4): mobile alkyl carbons (0–25 ppm), rigid alkyl carbons (25–46 ppm), carbons in primary and secondary alcohols, ethers and amines (60–90 ppm), acetalic C in carbohydrates and carbons in quaternary condensed tannins (90–110 ppm) not substituted by aromatic carbons, or having alkyl substituents (110–140 ppm), hetero-substituted aromatic carbons (140–160 ppm), carbonyl and carboxyl carbons, esters and carbonyl amides (160–190 ppm), and carbon in aldehydes and ketones (190–220 ppm) (Wilson 1987; Preston 1996; Skjemstad et al. 1997; Hu et al. 2000).

Comparing the CPMAS NMR spectra of samples F1 (unaltered) and F2 (severely affected by the fire), a clear indication of the fire's impact is given by the high contribution of aromatic carbons in the latter (F2, CPMAS, Fig. 1). When comparing the CPMAS NMR spectra of F3 and F4, the impact of fire is not as intense as in F2. A detailed assessment of the differences observed in the various spectral regions is as follows:

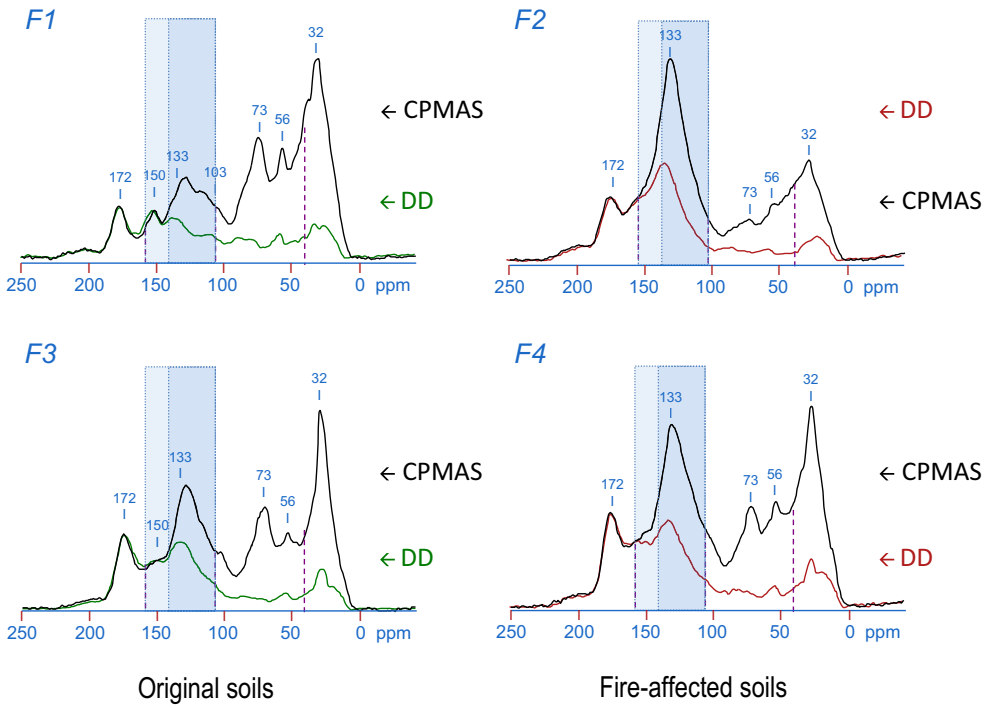

Fig. 1 Comparison of the solid-state ^{13}C NMR spectra of the HAs from the soils before and after the wildfires acquired under cross-polarization conditions (CPMAS) as well as their counterparts obtained with the dipolar dephasing (DD) pulse sequence. Regions for unsubstituted and *O*-substituted aromatic structures are marked in *shadowed boxes*. *Dashed lines* represent the integrated areas in Table 3

Table 3 Chemical shifts, integration values (%), and ratios between the main regions and subregions in the ^{13}C NMR spectra of humic acids. Tentative assignments of the main peaks at the different chemical shift ranges

Sample	Acquisition mode, ratios	0–25 Al term[a]	25–46 Al rig[b]	0–46 Total alkyl	46–60 >CHN<	60–90 –CH_2OH –CH(OH)–	90–110 >C(O[c])O– C_{4a}[d]	46–110 Total *O/N*-alkyl	110–140 Ar–H (R)[e]	140–160 Ar–O	110–160 Total aromatic	160–190 –COOH –CONHR	190–220 –CHO –CO–	160–220 Total carbonyl	Al/Ar	*O/N*-Al/Al	*O/N*-Al/Ar	C=O/Ar
F1	CPMAS	8.7	24.8	33.5	10.9	20.0	7.1	38.0	15.4	5.5	20.9	6.2	1.4	7.6	1.6	1.1	1.8	0.4
F2	CPMAS	5.8	13.6	19.4	6.7	8.8	6.7	22.2	35.0	11.3	46.3	10.0	2.1	12.1	0.4	1.1	0.5	0.3
F3	CPMAS	5.7	20.7	26.4	8.2	16.9	7.4	32.5	22.5	7.5	30.0	9.8	1.3	11.1	0.9	1.2	1.1	0.4
F4	CPMAS	6.3	18.2	24.3	8.5	13.9	7.7	30.1	25.7	8.8	34.5	9.6	1.3	11.1	0.7	1.2	0.9	0.3
F1	DD	6.8	9.8	16.6	5.5	15.2	6.5	27.2	20.6	15.6	36.2	17.4	2.6	20.0	0.5	1.6	0.8	0.6
F2	DD	5.0	3.7	8.7	2.2	5.6	5.6	13.4	35.5	19.3	54.8	19.4	3.7	23.1	0.2	1.5	0.2	0.4
F3	DD	4.0	8.5	12.5	3.6	6.0	6.0	15.6	27.6	18.1	45.7	23.9	2.3	26.2	0.3	1.3	0.3	0.6
F4	DD	5.7	8.0	13.7	3.2	5.9	6.4	15.5	28.0	17.0	45.0	22.9	2.9	25.8	0.3	1.1	0.3	0.6
F1	Non-protonated/mobile	2.4	3.5	5.9	2.0	5.4	2.3	9.7	7.3	5.6	12.9	6.2	0.9	7.1				
	Protonated/rigid	6.3	21.3	27.6	8.9	14.6	4.8	28.3	8.1	-0.1	8.0	0.0	0.5	0.5				
	CH/C	2.6	6.1	4.7	4.6	2.7	2.1	2.9	1.1	-0.0	0.6	0.0	0.5	0.0				
F2	Non-protonated/mobile	2.6	1.9	4.5	1.1	2.9	2.9	6.9	18.3	9.9	28.2	10.0	1.9	11.9				
	Protonated/rigid	3.2	11.7	14.9	5.6	5.9	3.8	15.3	16.7	1.4	18.1	0.0	0.2	0.2				
	CH/C	1.2	6.1	3.3	4.9	2.0	1.3	2.2	0.9	0.14	0.6	0.0	0.1	0.0				
F3	Non-protonated/mobile	1.6	3.5	5.1	1.5	2.5	2.5	6.4	11.3	7.4	18.7	9.8	0.9	10.7				
	Protonated/rigid	4.1	17.2	21.3	6.7	14.4	4.9	26.1	11.2	0.1	11.3	0.0	0.4	0.4				
	CH/C	2.5	4.9	4.1	4.5	5.87	2.0	4.1	1.0	0.0	0.6	0.0	0.4	0.0				
F4	Non-protonated/mobile	2.4	3.4	5.7	1.3	2.5	2.7	6.5	11.7	7.1	18.9	9.6	1.2	10.8				
	Protonated/rigid	3.9	14.8	18.6	7.2	11.4	5.0	23.6	14.0	1.7	15.6	0.0	0.1	0.3				
	CH/C	1.6	4.43	3.2	5.3	4.6	1.9	3.6	1.2	0.2	0.8	0.0	0.1	0.0				

R = Alkyl

[a] Alkyl terminal groups,

[b] Rigid alkyl C: alkyl CH_2, CH, and quaternary C,

[c] Anomeric C in carbohydrates,

[d] C_{4a}: C non-protonated (C_{4a}) in condensed tannins,

[e] Ar-H (R): C aromatic non-substituted and alkyl-substituted

Sample abbreviations are indicated in the "Materials and Methods" section

Table 4 Total abundances [a] of compounds identified by Py-GC-MS in soil humic acids

No.	Compound	MW	F1	F2	F3	F4	No.	Compound	MW	F1	F2	F3	F4
1	Pentene	70	0.45	0.00	0.30	0.00	45	Guaiacylacetone	180	1.45	0.00	0.52	0.25
2	Hexene	84	0.00	1.13	0.41	0.00	46	Vinylsyringol	180	0.00	0.00	0.00	0.14
3	Toluene	92	5.10	0.00	1.96	7.53	47	Ethylsyringol	182	0.00	0.00	0.00	0.14
4	Phenol	94	3.00	8.54	1.93	8.29	48	Tridecene	182	0.00	1.71	0.60	0.33
5	Heptene	98	0.00	5.06	0.49	0.33	49	*n*-Tridecane	184	0.00	0.76	0.41	0.36
6	Styrene	104	1.82	5.09	1.14	3.95	50	C_3-Alkylnaphthalenols	186	0.00	0.00	0.54	2.64
7	Xylene	106	3.47	6.74	0.71	0.94	51	C_4-Tetralins	188	0.42	0.00	0.11	0.76
8	Cresol	108	0.45	12.44	0.11	3.22	52	Propenylsyringol	194	0.00	0.00	0.00	0.14
9	Octene	112	0.00	0.85	0.35	0.33	53	Tetradecene	196	0.00	0.82	0.65	0.94
10	Indene	116	0.20	0.98	0.24	0.47	54	*n*-Tetradecane	198	0.00	0.64	0.35	0.54
11	C_3-Alkylbenzenes	120	3.70	3.78	1.44	3.66	55	Pentadecene	210	0.00	0.98	0.73	0.25
12	Vinylphenol	120	0.27	0.52	0.33	0.33	56	*n*-Pentadecane	212	0.00	0.52	0.46	0.47
13	C_2-Alkylphenols	122	2.32	1.34	0.00	1.30	57	Hexadecene	224	0.00	0.73	2.28	0.00
14	Guaiacol	124	15.67	10.61	3.88	3.44	58	*n*-Hexadecane	226	0.00	1.22	1.49	2.14
15	Nonene	124	0.00	1.40	0.00	0.33	59	Tetradecanoic acid	228	7.97	0.58	1.96	3.88
16	Naphthalene	128	0.00	0.85	0.00	0.11	60	Retene	234	0.37	2.04	0.00	0.40
17	*n*-Nonane	128	0.00	1.40	0.79	0.25	61	1,1′-bis (*p*-ethylphenyl) ethane	238	0.70	0.43	0.00	0.00
18	Methylindenes	130	0.70	0.40	0.19	0.94	62	Heptadecene	238	0.00	0.24	0.84	0.47
19	Tetralin	132	0.90	0.00	0.00	0.00	63	*n*-Heptadecane	240	0.00	0.61	0.68	0.47
20	C_4-Alkylbenzenes	134	1.32	0.64	0.62	1.30	64	*anteiso*-C_{15} fatty acid	242	0.00	0.00	0.79	0.36
21	C_3-Alkylphenols	136	2.10	0.00	0.41	2.46	65	*iso*-C_{15} fatty acid	242	0.00	0.00	0.49	0.22
22	Methylguaiacol	138	5.30	0.30	0.90	1.56	66	Pentadecanoic acid	242	0.00	0.00	0.60	1.01
23	Decene	140	0.00	1.43	0.52	0.47	67	Octadecene	252	0.00	0.34	1.14	0.58
24	C_1-Alkylnaphthalenes	142	0.30	3.11	0.65	0.72	68	Norabietatetraene	254	0.47	1.13	0.00	0.18
25	*n*-Decane	142	0.00	0.61	0.41	0.58	69	*n*-Octadecane	254	0.00	0.73	1.03	0.80
26	C_2-Alkylindenes	144	5.00	0.98	0.30	0.94	70	Hexadecanoic acid	256	9.95	1.01	9.34	14.67
27	C_5-Alkylbenzenes	148	0.00	0.18	0.68	0.47	71	C_{10}-Alkyloctahydroindene	264	0.00	0.00	14.34	0.87
28	Vinylguaicol	150	8.62	0.46	1.74	2.10	72	Nonadecene	266	0.22	0.18	1.33	0.65
29	Ethylguaiacol	152	2.90	0.03	0.95	0.47	73	*n*-Nonadecane	268	0.12	0.58	0.84	0.72
30	Syringol	154	0.00	0.00	0.00	1.01	74	Dehydroabietane	270	0.77	0.00	0.00	0.00
31	Undecene	154	0.00	1.56	0.79	0.69	75	Kaurene	272	1.42	0.00	0.00	0.00
32	C_2-Alkylnaphthalenes	156	0.82	1.98	0.19	0.94	76	Eicosene	280	0.00	0.18	0.92	0.14
33	*n*-Undecane	156	0.00	1.25	0.57	0.43	77	*n*-Eicosane	282	0.00	0.73	0.76	0.76
34	C_3-Alkylindenes	158	0.45	0.27	0.19	0.51	78	Octadecanoic acid	284	0.00	0.18	0.00	0.00
35	C_6-Alkylbenzenes	162	0.00	0.00	0.00	0.33	79	*n*-Heneicosane	296	0.00	0.37	0.00	0.00
36	C_5-Alkylphenols	164	1.77	0.00	0.00	0.00	80	*n*-Pentacosane	352	0.00	0.00	1.28	1.09
37	Propenylguaiacol	164	5.95	0.85	2.99	1.99	81	Steroid	368	0.00	1.37	0.43	0.47
38	Acetoguaiacone	166	0.00	0.00	0.87	0.94	82	Steroid	394	0.00	0.00	7.22	0.43
39	Propylguaiacol	166	0.32	0.00	0.00	0.14	83	Steroid	394	0.00	0.00	16.30	0.00
40	Dodecene	168	0.00	0.98	0.00	0.76	84	Steroid	396	0.00	0.00	0.27	3.48
41	Methylsyringol	168	0.00	0.00	0.00	0.91	85	Steroid	396	0.00	0.00	1.63	0.83
42	C_3-Alkylnaphthalenes	170	2.20	2.90	1.20	1.52	86	Steroid	396	0.00	0.00	0.00	1.70
43	C_2-Alkylnaphthalenols	172	0.42	0.00	0.00	0.00	87	Steroid	410	0.00	3.23	1.44	0.00
44	C_3-Tetralins	174	0.57	0.00	0.00	0.00							

[a] Percentage relative to the chromatographic area for the peaks considered. Only chromatographic peaks representing more than 0.5% of the total volatile products were considered

3.1.1 Alkyl region (0–46 ppm)

This region includes signals assigned to saturated hydrocarbons, from primary to quaternary, including alkanes and most alkyl groups. In the case of HAs, these signals can be attributed to methylene C in organic acids such as fatty acids or peptide structures. Some may derive from fatty acids, waxes, resins, cutans, suberans, or condensed C–C networks in alkyl domains which were co-extracted with the humic material. Table 3 shows that the contribution of alkyl carbons varies from 19 to 33% of the total carbon. Comparing the CPMAS and DD ^{13}C NMR spectra allows distinguishing between alkyl carbons, in short and medium chain structures and alkyl carbons present in long chains with high flexibility (Kögel-Knabner 1993) or mobile terminal methyl groups. The region between 25 and 46 ppm is often ascribed to CH_2, CH, and quaternary C whereas signal intensity in the 0–25 ppm region is typically for CH_3 and some CH_2. All spectra reveal an important quantitative contribution of both types of alkyl C. Considering the high-intensity loss of the total alkyl C region during dipolar dephasing, some prevalence of protonated or rigid components may be assumed. Note that for both sample sets, the fire event yielded in a decrease of the ratio between fast dephasing C and slowly dephasing C (CH/C) in the chemical shift region between 0 and 46 ppm which is best explained with a decrease of compounds with comparatively longer alkyl chains and thus a relative increase of mobile terminal methyl C.

3.1.2 Region 46–110 ppm

Signals in the chemical shift region between 60 and 90 ppm correspond to the C_2–C_5 and C_6 (secondary and primary alcohols) from carbohydrate-derived structures. During charring, such structures are strongly affected and quickly transformed into furans and benzenic units which are expressed by a relative decrease of the signal intensity between 60 and 90 ppm with a concomitant increase of contributions in the chemical shift region of aromatic C. In our study, this alteration was more expressed for the sample set F1 and F2 than for F3 and F4. The region between 46 and 60 ppm includes signals from methoxyl carbons but also from N-substituted alkyl C such as the Cα of amino acids. The DD spectra help to infer the quantitative contribution of these constituents: when produced by CH_3O, some intensity will remain after dephasing for 60 μs, whereas it vanishes when it derives from R–CH(COOH)(NH_2) (Preston 1996). As indicated in Table 3, in our samples, most of the intensity in this region is assignable to *N*-alkyl C. The slight increase of the CH/C ratio of this region at both sites after the fire may point towards a preferential degradation of CH_3O, possibly due to the removal of this group from lignin residues during fire.

3.1.3 Region 90–110 ppm

In the region between 90 and 110 ppm (centered in 103 ppm), the intensity can be assigned to anomeric C (C_1) of carbohydrates and to quaternary carbons (C_{4a}) of condensed tannins (Fig. 1). If the signal derives from condensed tannins, its intensity should remain unchanged in the DD spectrum (Wilson and Hatcher 1988; Preston 1996). In our spectra, approximately a half of the intensity in this region survives dipolar dephasing, irrespective of the fire history. However, here one has to bear in mind that e.g., fructose may contribute to the low dephasing carbon pool.

3.1.4 Aromatic region (110–160 ppm)

Aside from aromatic carbons, this region includes signals corresponding to olefinic carbons. Protonated and alkyl-substituted aromatic C give signals between 110 and 140 ppm. According to our DD spectra, approximately 50% of the aromatic C contributing to this chemical shift region are protonated. Hetero-subtituted carbons produce signals in the chemical shift region between 140 and 160 ppm. Some signal intensity may be ascribed to lignin: 145–150 ppm signals from the C_3 and C_4 (Maciel et al. 1985). However, after charring of carbohydrates, Cα of furans will also contribute to the region between 140 and 160 ppm. The signals of the respective Cβ are found between 110 and 120 ppm. Whereas, the ratio *O/N*-alkyl C-to-alkyl C showed no major alteration by fire, a clear decrease was observed for the alkyl C-to-aryl C and *O/N*-alkyl C/aryl C ratios in the spectra of the HA from the soil under burnt forest F2 as regards to its control sample F1.

3.1.5 Carbonyl region (160–220 ppm)

This region includes signals from carboxyl acids in esters, amides, aldehydes, and ketones, the latter producing signals of small intensity between 185 and 200 ppm. Although charring is expected to lead to decarboxylation, no considerable decrease of its relative contribution to the total C of the HA from the burnt soils relative to the unburnt counterpart was revealed. However, here one has to bear in mind that the standard isolation procedure for HAs extracted only substances which are soluble in aqueous solution at high pH. Thus, only oxidized or partially oxidized black carbon residues were extracted with our approach.

3.2 Study by pyrolysis-gas chromatography-mass spectrometry

The major pyrolysis products are listed in Table 4. The main series detected corresponded to alkylbenzenes, methoxyphenols, alkylphenols, *n*-alkanes, *n*-alkenes, fatty acids and steroids (Tinoco et al. 2002; Miralles et al. 2015).

Major peaks for C_3–C_6 alkylbenzenes (compounds 11, 20, 27, and 35, as different isomers) are present. Also, several polycyclic compounds such as indene (compound 10), alkylindenes (C_1–C_3, 20, 26, and 34), naphthalene (compound 16), and alkylnaphthalenes (C_1–C_3, 24, 32 and 42) were found. Different fatty acids were identified from their m/z 60 ion trace (mainly even-C homologs from C_{14} to C_{18}, the major compounds being 59, 66, 70, and 78). Pyrolysis also released typical *iso*-pentadecanoic and *anteiso*-pentadecanoic acids (compounds 64 and 65, respectively). The total abundance of *n*-alkanes (C_9–C_{26}) amounted to 0.1–9.4%, whereas that for alkenes (C_5–C_{22}) ranged between 0.7–17.6%.

Phenolic compounds (2.8–23.3%) were major pyrolysis compounds. They included phenol (compound 4), vinylphenol (compound 12), C_1–C_5 alkylphenols, and several methoxyphenols with typical lignin origin. Phenol (compound 4) and cresol (compound 8) reflect the contribution of lignin and proteins (Saiz-Jiménez and de Leeuw 1986a, b).

The semi-quantitative information of the pyrograms was represented as surface density plots (Fig. 2). Such a plot displays the total abundances per unit area distributed over a surface. In this way, the third dimension in the space defined by the atomic H/C and O/C values is a function of both the abundance of the individual molecules and their proximity in the basal plane (i.e., not only the abundances of isomer compounds are aggregated but also compounds with similar H/C and O/C ratios coincided in the same cell of the discrete 50 × 50 matrix). The resulting 3D plot (Fig. 2) shows well-defined, mountain-like broad peaks corresponding to clusters of compounds with similar stoichiometry. Increasing the number of smoothing iterations (moving average, e.g., 3 in Fig. 2) leads to decreased "resolution" (poor displaying of small-size, sharp compound clusters, or individual molecules behaving at outliers), but alternatively shows a more simplified 3D plot illustrating the presumptively "major" macromolecular domains.

At first glance, the major compound domains are well-defined in terms of the H/C and O/C ratios, i.e., aromatic and aliphatic compounds are clearly separated as isolated clusters or 3D peaks, in the latter case embracing mainly alkanes, olefins, and fatty acids. The intermediate regions of the H/C axis include clusters for terpenoids, steroids, and other hydroaromatic compounds, whereas well-defined clusters for series of alkylbenzenes and progressively condensed polycyclic

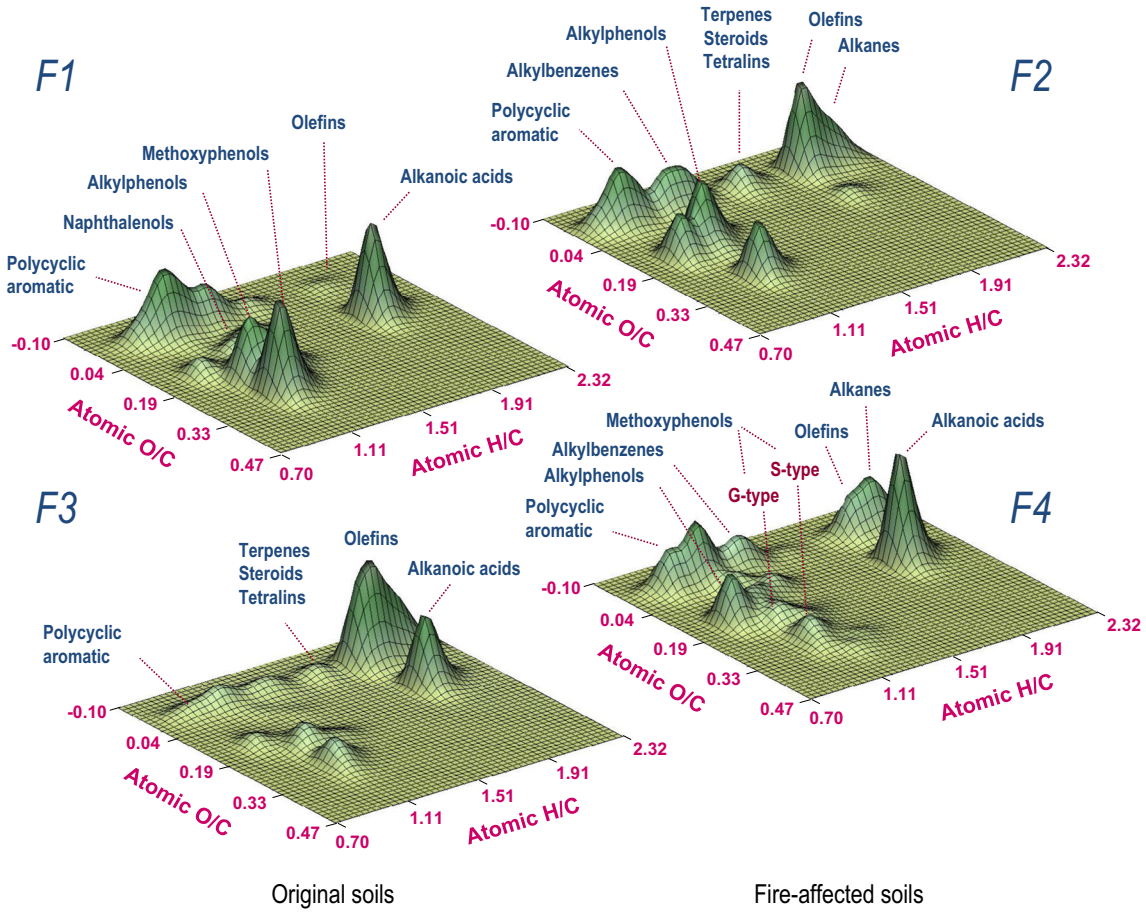

Fig. 2 Surface density map displaying cumulative abundances of HA pyrolysis compounds represented in the space defined by their H/C and O/C atomic ratios in a classical Van Krevelen's (1950) diagram

aromatic hydrocarbons are seen at H/C values < 1.1. Considering the *O*-containing compounds, the most conspicuous clusters formed were those for phenols, methoxyphenols, and alkylnaphthalenols. In particular, the differences between guaiacyl and syringyl compounds are evident in the plot as separate clusters.

A valuable feature of the interpretation of the pyrolysis results from the surface density plots is that the changes in the molecular composition of the HAs are straightforwardly evident after visual inspection (Fig. 2). Classical fire-induced effects (e.g., dehydration, decarboxylation, demethylation, aromatization, and increase in chemical diversity after accumulation of newly-formed cyclic or polycyclic compounds) (González-Pérez et al. 2004; Jiménez-Morillo et al. 2016a) are evident as changes in the position and size of the major clusters. In fact, in Fig. 2, progressive aromatization and condensations are quickly recognized as the "shifting" of the major clusters towards the origin of coordinates. In order to illustrate changes in aromaticity (i.e., generation of pyrogenic polycyclic compounds), we consider that this presentation of the cumulative results is more structurally meaningful than e.g., calculating classical families of compounds: phenanthrenes, naphthalenes, benzenes, phenols, etc. Due to these series of homologs include alkyl substitutions (in this case and in general from C_1 to C_5), the changes in aromaticity and condensation are accurately shown by the size of the clusters. For instance, alkyl-substituted 3-ring compounds may have larger H/C ratio than the dealkylated 2-ring counterparts (may share the same coordinates in the H/C–O/C plane), and therefore the accumulation of pyrogenic aromatic material is properly reflected by the "shifting" of the cluster peaks towards the origin of coordinates.

The comparison in Fig. 2 of the surface plots for HAs from the control and fire-affected soils shows clearly the different response of the pyrolysis products in terms of the intensity of the fires: high-intensity fire (F1–F2) and low or medium intensity (F3–F4).

The differences between the soil organic matter quality in the unburnt forests (F1 and F3) were also evident in the surface plots and probably contributed to the comparatively severe effects of the fire on the HAs from the former forest (F1: semiarid conditions and thick litter layer almost exclusively consisting of dry pine needles, which was probably associated to the large yields of methoxyphenols indicating accumulation of non-decomposed lignin in the HAs) as regards to forest F3 (moist mountain forest with herbaceous layer and humic substances at advanced stages of diagenetic transformation). These differences in F3 soil are probably reflected in the lower yields of methoxyphenols and dominance of olefins, the latter consistent with macromolecular rigid alkyl domains incorporated into the structure of the HA (Fig. 2).

In the high-intensity fire (F1–F2), a clear rearrangement of the HA alkyl domain is observed in which fatty acids are selectively volatilized by thermoevaporation or previous in-chain cracking. Nevertheless, decarboxylation of fatty acids leading to fire-recalcitrant alkanes and olefins, or the selective concentration of preexistent recalcitrant polymethylene structures is also suggested by the plot. This phenomenon is not unusual and has often been related to increased water repellence of soils after the fire's effect (DeBano 2000; Graber et al. 2009; Jiménez-Morillo et al. 2016b and references therein). Changes in the polycyclic aromatic region are also evident as a result of fire, suggesting aromatization and increasing ring condensation (Almendros et al. 2003). In addition, hydroaromatic products also accumulated after fires, and the prevalence of phenols over methoxyphenols (mostly of the guaiacyl-type, as correspond to the pine vegetation) was also observed.

In the medium-intensity fire (F3–F4) event, there is a clear increase of compounds of a very low H/C ratio, which is interpreted of accumulation of newly-formed (or diagenetically transformed) polycyclic aromatic structures (González-Pérez et al. 2004, 2014; Almendros et al. 1992). Nevertheless, the total aromaticity also increases in relative terms due to the probable selective preservation not only of structures yielding alkylphenols upon pyrolysis but also methoxyphenols. As some differences to the high-intensity fire (leading to severe selective depletion of most compound types), in this case, it was more evident: (a) some resilience of alkyl constituents including acids and (b) outstanding quantitative and qualitative increase in chemical diversity of aromatic compounds (i.e., fire does not lead to simplification of the molecular assemblages from HAs, but to accumulation of newly-formed structures in addition to preservation of other aromatic compounds that in the unburnt sample represents minor compounds).

4 Conclusions

a) Dipolar dephased ^{13}C NMR spectra of the studied HAs provided specific information on the degree of aromatic substitution, which could be useful in the appraisal of pyrogenic structures in HAs from fire-affected soils. The DD ^{13}C NMR spectra of the HAs from fire-affected soils confirm medium-size domains of newly-formed aromatic rings. Considerable signal intensity in the chemical shift region of *O*-aryl C indicates the presence of furans. Nevertheless, the accumulation of "secondary aromatic structures" was only evident in recent, high-intensity wildfire, whereas CPMAS and DD spectra of HAs from soils after moderate burning indicated mainly internal rearrangements of the whole aliphatic domain, reflected by the decrease of the *O/N*-alkyl/alkyl ratio.
b) The analysis of the Py-GC/MS data clearly show the different responses of the pyrolysis products in terms of the

intensity of the fires: total abundances of polycyclic aromatic hydrocarbons showed a systematic enhancement as results of burning, whereas proportions of *O*-containing aromatic products (e.g., phenols and naphthalenols) tend to increase after a medium-intensity fire where inputs from plant charred material are observed on the soil.

c) New "surface density plots" based in the classical Van Krevelen intuitive graphical-statistical method were found useful for the rapid interpretation of semiquantitive differences between complex Py-GC/MS molecular assemblages from samples representative of different environmental situations. In fact, the unsupervised formation of clusters or 3D peaks including compounds with similar atomic ratios is helpful to monitor the changes in aromaticity, demethoxylation, and oxidation, at least compared to the supervised, time-consuming calculation of cumulative values for homologous series of compounds according to conventional criteria of chemical nomenclature. The resulting patterns of compound clusters formed in the space defined by its atomic ratios reflected the main molecular fire-induced transformations in soil HAs after high- or medium-intensity wildfires in a natural scenario.

Acknowledgements The contributions by three anonymous reviewers and the financial support by the Spanish CICyT (grant CGL2013-43845-P) are gratefully acknowledged.

References

Alemany LB, Grant DM, Alger TD, Pugmire RJ (1983) Cross polarization and magic angle sample spinning NMR spectra of model organic compounds. 3. Effect of the ^{13}C-^{1}H dipolar interaction on cross polarization and carbon-proton dephasing. J Am Chem Soc 105:6697–6704

Almendros G, González-Vila FJ (2012) Wildfires, soil carbon balance and resilient organic matter in Mediterranean ecosystems. A review. Spanish J Soil Sci 2:8–33

Almendros G, Knicker H, González-Vila FJ (2003) Rearrangement of carbon and nitrogen forms in peat after progressive thermal oxidation as determined by solid-state ^{13}C- and ^{15}N spectroscopy. Org Geochem 34:1559–1568

Almendros G, González-Vila FJ, Martin F, Fründ R, Lüdemann H-D (1992) Solid state NMR studies of fire-induced changes in the structure of humic substances. Sci Total Environ 118:63–74

Conte P, Spaccini R, Piccolo A (2004) State of the art of CPMAS ^{13}C-NMR spectroscopy applied to natural organic matter. Prog Nucl Mag Res Spectrosc 44:215–223

Czimczik C, Preston CM, Schmidt MWI, Werner RA, Schulze E-D (2002) Effects of charring on mass, organic carbon, and stable carbon isotope composition of wood. Org Geochem 33:1207–1223

DeBano LF (2000) The role of fire and soil heating on water repellency in wildland environments: a review. J Hydrol 231/232:195–206

Duchaufour P (1987) Manual de Edafología. Masson, Barcelona, p 224

Fründ R, Lüdemann H-D (1989) The quantitative analysis of solution- and CPMAS-C-13 NMR spectra of humic material. Sci Total Environ 81/82:157–168

González-Pérez JA, Almendros G, De la Rosa JM, González-Vila FJ (2014) Appraisal of polycyclic aromatic hydrocarbons (PAHs) in environmental matrices by analytical pyrolysis (Py-GC/MS). J Anal Appl Pyrolysis 109:1–8

González-Pérez JA, González-Vila FJ, Almendros G, Knicker H (2004) The effect of fire on soil organic matter—a review. Environ Intern 30:855–870

Graber ER, Tagger S, Wallach R (2009) Role of divalent fatty acid salts in soil water repellency. Soil Sci Soc Amer J 73:541–549

Hatcher PG (1987) Chemical structural studies of natural lignin by dipolar dephasing solid-state ^{13}C nuclear magnetic resonance. Org Geochem 11:31–39

Hatcher PG, Schnitzer M, Vassallo AM, Wilson MA (1989) The chemical structure of highly aromatic humic acids in three volcanic ash soils as determined by dipolar dephasing NMR studies. Geochim Cosmochim Acta 53:125–130

Hu WG, Mao JD, Xing BS, Schmidt-Rohr K (2000) Poly(methylene) crystallites in humic substances detected by nuclear magnetic resonance. Environ Sci Technol 34:530–534

Jiménez-Morillo NT, de la Rosa JM, Waggoner D, Almendros G, González-Vila FJ, González-Pérez JA (2016a) Fire effects in the molecular structure of organic matter in soil size fractions under *Quercus suber* cover. Catena 145:266–273

Jiménez-Morillo NT, González-Pérez JA, Jordán A, Zavala LM, de la Rosa JM, Jiménez-González M, González-Vila FJ (2016b) Organic matter fractions controlling soil water repellency in sandy soils from the Doñana national park (SW Spain). Land Degrad Develop 27:1413–1423

Knicker H (2007) How does fire affect the nature and stability of soil organic nitrogen and carbon? A review. Biogeochemistry 85:91–118

Knicker H (2011) Solid state CPMAS ^{13}C and ^{15}N NMR spectroscopy in organic geochemistry and how spin dynamics can either aggravate or improve spectra interpretation. Org Geochem 42:867–890

Knicker H, González-Vila FJ, Polvillo O, González-Pérez JA, Almendros G (2005) Fire-induced transformation of C- and N-forms in different organic soil fractions from a dystric Cambisol under a Mediterranean pine forest (*Pinus pinaster*). Soil Biol Biochem 37: 701–718

Kögel-Knabner I (1993) Biodegradation and humification processes in forest soils. In: Bollag JM, Stotzky G (eds) Soil biochemistry, vol 8. Dekker, New York, pp. 101–135

Kramer RW, Kujawinski EB, Hatcher PG (2004) Identification of black carbon derived structures in a volcanic ash soil humic acid by Fourier transform ion cyclotron resonance mass spectrometry. Environ Sci Technol 38:3387–3395

Maciel GE, Haw JF, Smith DH, Gabrielsen BC, Hatfield GR (1985) Carbon-13 nuclear magnetic resonance of herbaceous plants and their components, using cross polarization and magic-angle spinning. J Agric Food Chem 33:185–191

Miralles I, Piedra-Buena A, Almendros G, González-Vila FJ, González-Pérez JA (2015) Pyrolytic appraisal of the lignin signature in soil humic acids: assessment of its usefulness as carbon sequestration marker. J Anal Appl Pyrolysis 113:107–115

Monnier G, Turc L, Jeanson-Luusinang C (1962) Une méthode de fractionnement densimétrique par centrifugation des matières organiques du sol. Ann Agron 13:55–63

Preston CM (1996) Applications of NMR to soil organic matter analysis: history and prospects. Soil Sci 161:144–166

Saiz-Jiménez C, de Leeuw JW (1986a) Chemical characterization of soil organic matter fractions by analytical pyrolysis-gas chromatography-mass spectrometry. J Anal Appl Pyrolysis 9:99–119

Saiz-Jiménez C, de Leeuw JW (1986b) Lignin pyrolysis products: their structures and their significance as biomarkers. Org Geochem 10:869–876

Skjemstad JO, Clark P, Golchin A, Oades HM (1997) Characterization of soil organic matter by solid state ^{13}C NMR spectroscopy. In: Cadisch G, Giller KE (eds) Driven by nature: plant litter quality and decomposition. CAB International, Wallingford, pp. 253–271

Smernik RJ, Oades JM (2001) Solid-state ^{13}C-NMR dipolar dephasing experiments for quantifying protonated and non-protonated carbon in soil organic matter and model system. Eur J Soil Sci 52:103–120

Stevenson FJ (1994) Humus chemistry. Genesis, composition, reactions. Wiley, New York, p. 512 ISBN: 978-0-471-59474-1

Tinoco P, Almendros G, González-Vila FJ (2002) Impact of the vegetation on the lignin pyrolytic signature of soil humic acids from Mediterranean soils. J Anal Appl Pyrolysis 64:407–420

Van Krevelen DW (1950) Graphical-statistical method for the study of structure and reaction processes of coal. Fuel 29:269–284

Walkley A, Black IA (1934) An examination of the Degtjareff method for determining soil organic matter, and a proposed modification of the chromic acid titration method. Soil Sci 37:29–38

Wilson MA (1987) NMR techniques and applications in geochemistry and soil chemistry. Pergamon, Oxford, p. 352 ISBN-13:978-0080348520

Wilson MA, Hatcher PG (1988) Detection of tannins in modern and fossil barks and in plant residues by high-resolution solid-state ^{13}C nuclear magnetic resonance. Org Geochem 12:539–546

WRB (2006) World Reference Base for soil resources 2006. World soil resources reports 103. FAO, Rome